Multimedia Tools and Applications
https://doi.org/10.1007/s11042-024-19974-3

Discrete ripplet-II transform feature extraction and metaheuristic-optimized feature selection for enhanced glaucoma detection in fundus images using least square-support vector machine

Santosh Kumar Sharma[1] · Debendra Muduli[1] · Adyasha Rath[1] · Sujata Dash[2] · Ganapati Panda[1] · Achyut Shankar[3,4,5,6,7] · Dinesh Chandra Dobhal[7]

Received: 15 December 2023 / Revised: 13 June 2024 / Accepted: 11 July 2024

Abstract
Recently, significant progress has been made in developing computer-aided diagnosis (CAD) systems for identifying glaucoma abnormalities using fundus images. Despite their drawbacks, methods for extracting features such as wavelets and their variations, along with classifier like support vector machines (SVM), are frequently employed in such systems. This paper introduces a practical and enhanced system for detecting glaucoma in fundus images. The proposed model adresses the chanallages encountered by other existing models in recent litrature. Initially, we have employed contrast limited adaputive histogram equalization (CLAHE) to enhanced the visualization of input fundus inmages. Then, the discrete ripplet-II transform (DR2T) employing a degree of 2 for feature extraction. Afterwards, we have utilized a golden jackal optimization algorithm (GJO) employed to select the optimal features to reduce the dimension of the extracted feature vector. For classification purposes, we have employed a least square support vector machine (LS-SVM) equipped with three kernels: linear, polynomial, and radial basis function (RBF). This setup has been utilized to classify fundus images as either indicative of glaucoma or healthy. The proposed method is validated with the current state-of-the-art models on two standard datasets, namely, G1020 and ORIGA. The results obtained from our experimental result demonstrate that our best suggested approach DR2T+GJO+LS-SVM-RBF obtains better classification accuracy 93.38% and 97.31% for G1020 and ORIGA dataset with less number of features. It establishes a more streamlined network layout compared to conventional classifiers.

Keywords IOP · ONH · CLAHE · GJO · DR2T · LS-SVM

1 Introduction

Glaucoma is an ophthalmic disorder that affects the optic nerve (ON), resulting in an anomaly in the eye's drainage system. This can lead to fluid buildup, resulting in increased pressure that possesses the capability to harm the optic nerve. This leads to a distinct optic nerve head appearance during fundoscopic evaluation and a corresponding gradual decline in vision.

Extended author information available on the last page of the article

Published online: 10 September 2024

For the preservation of life, early screening detection is crucial to prevent the loss of vision. Approximately four million individuals in the United States are believed to suffer from glaucoma, with half unaware of their condition. Out of these, around 120,000 have experienced blindness due to glaucoma, constituting about 9% to 12% of all cases of blindness in the country. Elevated intraocular pressure (IOP) affects approximately 2% of those aged between 40 and 50 and about 8% of individuals aged over 70 [46]. Hence, it is imperative to include glaucoma screening as an integral aspect of continuous healthcare. The primary methods for detecting glaucoma encompass evaluating intraocular pressure (IOP) [12], conducting visual field tests [13], and analyzing the configuration of the optic nerve head (ONH) [14]. Numerous research endeavours have created computer-aided diagnosis (CAD) systems to identify glaucoma early. Gautam et al. [15] presented a novel ML approach to Glaucoma detection method that combines FAWT, texture analysis, PCA, and SVM classification on Fundus images for efficient diagnosis. Certain illnesses result in minor issues with the human eye, while others can result in permanent vision loss. Hence, developing a CAD system specialized for classifying glaucoma in human eyes through fundus images, which automates the work of an ophthalmologist, is of utmost importance. It plays a crucial part in making accurate and timely clinical judgments. Fundus images, an advanced method in retina imaging, are commonly utilized for acquiring fundus images of the glaucoma-affected fundus due to their capacity to efficiently transform data associated with eye conditions in the human eye [44]. Hence, when the ON sustains damage, the connection in the eye disrupts the brain. In addition, glaucoma is a non-invasive imaging technique that doesn't require invasive procedures or expose the patient to radiation, unlike other options like CT scans and X-rays. Examining fundus images manually for this detection takes considerable time, is an expensive, inconvenient process, and is a complicated scheme that requires expert supervision. To tackle these difficulties, developing a CAD model using a dedicated computing system is crucial. This system can assist ophthalmologists in making faster and more accurate judgments by integrating multiple algorithms to process retinal images and recognize patterns at various points.

Researchers have noted that DWT is primarily deployed to extract image-processing feature tools. This application involves identifying features in fundus images across various scales while addressing singularities in one-dimensional (1D) data [21]. Hence, defining two-dimensional (2D) singularities, like the boundaries of fundus images, has proven to be a challenging task with limited precision [32]. So, DWT needs help to effectively capture curve-like characteristics in fundus images [41]. Hence, there is a significant need for enhanced changes to tackle these concerns. Therefore, the classifier, specifically the SVM, has been employed in detecting glaucoma based on CAD models due to its ability to discriminate between discrete input patterns and make predictions for continuous functions. Hence, The conventional SVM algorithm experiences increased computational intricacy and exhibits subpar performance when handling large datasets [49]. Moreover, specific fundus images necessitate more features, thereby complicating and increasing the burden on the classification task. This approach utilizes specific points of interest within a multi-dimensional feature space derived from fundus images, demonstrating robustness to changes in the area near the optic disc. Machine learning (ML) has been used to tackle various tasks involving the analysis of medical images, demonstrating impressive speed and efficiency in optimizing processes across a wide range of diseases, such as breast cancer diagnosis [26–31], diabetes detection [42, 43], glaucoma detection [44] etc.

From the article, we have developed an efficient CAD model that can tackle the difficulties faced by existing models. The deployed scheme has significantly improved by introducing the ripplet-II transform and a novel version of the least-square SVM (LS-SVM) with a list of kernels in our suggested system. The research study contributes explicitly in the following ways:

1. Utilizing the discrete ripplet-II transform (DR2T) for feature extraction offers benefits by effectively capturing two-dimensional irregularities and a group of curves in fundus images.
2. The golden jackal optimization (GJO) aimed to select the essential elements from the range of potential solutions to eliminate redundant and trivalent features and LS-SVM (GJO+LS-SVM) to classify better classification accuracy.
3. The LS-SVM acts as the classifier and provides a higher computational efficiency level than the conventional SVM.
4. Comparison with alternative capable techniques based on classification accuracy and quantity of attributes using three widely recognized datasets.

The remainder of this article is structured in the following manner: Section 2 summarises the literature regarding glaucoma detection. Section 3 comprehensively explains our approach, encompassing the suggested methodology scheme. In Section 4, the experimental findings were explored, and the results were assessed. This Section 5 highlights the summarization of the research's results and delineates possible directions for future research.

2 Related works

In contemporary methods for detecting glaucoma through categorization reliant on distinguishing features, the entire fundus image or a portion of the retina, including the optic disc, is employed for feature extraction. To extract and consolidate the methods and characteristics of significant advancements in utilizing machine learning (ML) to classify and diagnose glaucoma. In [52], the authors used an enhanced CAD scheme that experimented on four ocular conditions linked to an online platform through a cloud-based system, and SVM was used as a classifier for glaucoma detection. In [17], the authors used a new CAD system specified as contrast-limited adaptive histogram equalization (CLAHE) techniques to extract features from unlabeled datasets, which leads to avoiding overfitting problems. Maheswari et al. [24] have implemented new techniques for the detection of glaucoma by employing an empirical wavelet transform (EWT) to break down the list of images and extract correntropy features and used LS-SVM to detect glaucoma. In [25], have employed a new technique by utilizing the variational mode decomposition (VDM) technique for the decomposition of images; various aspects like Kapoor entropy, Renyi entropy, Yager entropy, and feature dimension are considered for extracting VDM model components., and employing LS-SVM for classification were applied. Kausu et al. [19] have employed features derived from the dual-tree complex wavelet transform, used fuzzy c-means clustering methods and Otsu's optic-cup segmentation thresholding. In [37], the authors have presented OD Localization in object detection involves employing the non-parametric GIST descriptor to minimize the application of locality sensitivity discriminant analysis (LSDA) via various feature selection and ranking approaches and classification. Parashar et al. [34] utilized a novel CAD approach to the diagnosis of glaucoma, employing wavelet analysis to break down fundus images into multiple modes. Subsequently, we extract fractal dimension (FD) and diverse entropy utilized for capture and construct an LS-SVM model based on various kernel functions. In [48], the authors have used a new CAD model employing machine learning methodologies, and a deep sparse autoencoder was introduced. This model was designed to amalgamate attributes from deep and primary features, improving the overall effectiveness of representing advanced features and potentially enhancing the efficiency of expressing high-level features. Furthermore, the model integrates L1 regularization to augment the synergy of deep features, especially in situations with a scarcity of sample data. Recent literature emphasizes the prominent role of machine learning, especially within ensemble learning methods. This is particularly beneficial in the biomedical domain, even when datasets are scarce. Many models rely on machine learning approaches, yet no prior research has concentrated on ensemble methods for classifying glaucoma. Therefore, our proposed study centres on ensemble learning, leveraging the combined power of XGBoost, SVM, and LR to achieve superior classification outcomes compared to conventional models. In [45], the authors employed an ELM classifier after utilizing DWT and HOG features. Additionally, Balasubramanian and Ananthamoorth [3], the authors deployed a novel CAD model is described, where correlation attributes are chosen through a bio-inspired algorithm, and a KELM classifier based on salp-swarm optimization is applied. In [23] introduced a scheme that utilizes speeded-up robust feature (SURF), histogram of oriented gradients (HOG) features. Based on the technique, we incorporated an improved version of the grey wolf optimization (GWO) method alongside an SVM as a classifier. Raja et al. [38] have extracted statistical features using hyper-analytic wavelet transformation (HWT). Furthermore, They applied a hybrid PSO method with a diverse particle population and employed an SVM to classify glaucoma diagnosis [42].

In the literature, most computer-aided diagnosis (CAD) models cannot provide a good classification result. Schemes in the literature have higher computational complexity and are unsuitable for real-time applications. Many existing CAD models rely on handcrafted feature extraction procedures. Almost all CAD approaches are focused on different machine-learning algorithms. Choosing the right features and effectively categorizing them has remained a crucial challenge.

3 Proposed methodology

Our employed scheme is based on four prime sections: preprocessing of fundus images, extraction of features, selection of features and classification. Figure 1 is viewed as an archi-

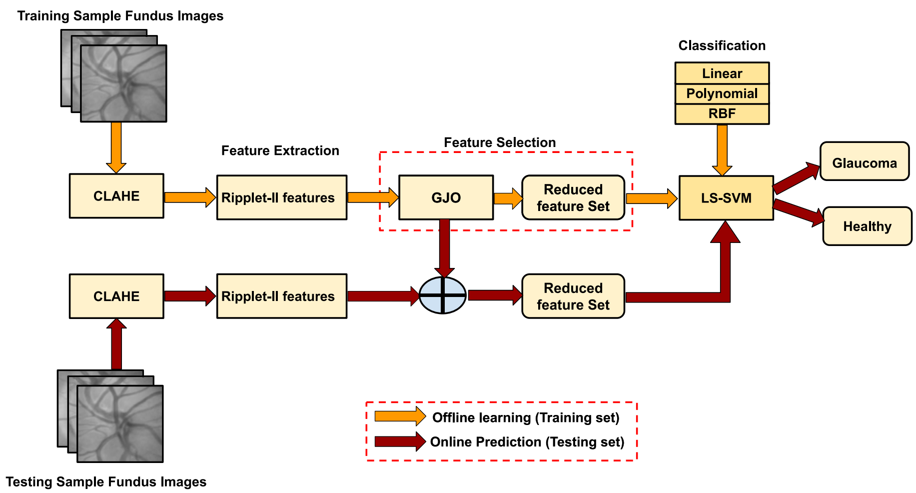

Fig. 1 Proposed CAD model for glaucoma classification

tectural scheme that employs an enhanced computer-aided diagnosis (CAD) model. Each section is described in detail.

3.1 Preprocessing

In our proposed research, we have divided the glaucoma datasets and Split the data into a training set comprising 60% and a testing set comprising 40% to attain the utmost accuracy. Our research focuses on two well-known datasets: G1020 [2] and ORIGA images [53]. To improve the quality of our dataset, we applied a cropping technique to find relevant regions of interest (ROI). Ophthalmologists provided the cup-to-disc(CDR) ratio based on numerous fundus images. Our approach primarily centred on cropped images resized at 256 × 256 pixels. In cases where specific ROIs were unavailable due to a lack of prior knowledge, the entire 256 × 256 image has been considered. We have specified sample images from both datasets illustrated in Fig. 2, and some sample image details are tabulated in Table 1.

3.1.1 Prepocessing based on CLAHE method

To establish a balance within the shared input space, we have employed contrast limited adaptive histogram equalization (CLAHE) technique, commonly used in image processing [36]. Unlike adaptive histogram equalization (AHE), CLAHE offers advantages such as avoiding excessive noise amplification and reducing the occurrence of edge-shadowing effects [35]. This method enhances image contrast by redistributing intensity values, making image details more distinguishable. Traditional histogram equalization can have drawbacks, such as amplifying noise and not considering local image characteristics. CLAHE addresses these issues by applying adaptive histogram equalization locally, ensuring that contrast enhancement is limited to a specified level.

3.2 Feature extracton using discrete ripple-II transform (DR2T)

In image processing, feature extraction involves distilling vital data from images to simplify their complexity, making them suitable for tasks like recognizing objects and analyzing patterns. This is achieved through edge detection and texture analysis, which help identify and depict significant image attributes.

The Fourier transform struggles with image feature extraction due to its inability to retain temporal information and handle 1D singularities, leading to ineffective edge depiction. It performs better with smoother features. In contrast, the wavelet transform is adept at

Fig. 2 Sample images of both datasets (G1020 and ORIGA)

Table 1 Proposed retinal image data sets(Glaucoma with Healthy)

Data sets	Total Images		Training Images		Testing Images	
	G	H	G	H	G	H
G1020	296	724	178	434	118	290
ORIGA	168	482	101	289	67	193

capturing 1D singularities but struggles with 2D singularities along arbitrary curves. To address the issue inherent in traditional wavelets, an alternative transformation known as the ridgelet transform was introduced. This transformation relies on the Radon transform and aims to provide a solution to the problem above [5, 11]. Ridgelet excels at identifying linear singularities but needs help with two-dimensional ones. To address this, Candes and Donoho introduced the initial curvelet transform, using a multiscale ridgelet approach to target smooth curve singularities in 2D. Afterwards, they introduced an improved version of the curvelet transform known as the fast discrete curvelet transform (FDCT). This version excels in simplicity, speed, and reduced redundancy compared to its predecessor [6]. Curvelet has recently garnered considerable attention due to its multi-resolution features, heightened directional sensitivity, anisotropy, and precise localization. Anisotropy ensures the resolution of 2D irregularities along smooth C2 curves, achieved through a scaling principle resembling a parabolic pattern [4]. However, the justification behind selecting parabolic scaling remains to be determined. To tackle this issue, a new transformation called the ripplet-I transform is introduced. This transformation expands the scalability principle's application [16, 51]. In ripplet-I, transform expands upon the idea of a curvelet transform by introducing two extra hyperparameters: the correlated parameter denoted as c and the degree of parameter denoted as d. Here, $c = 1 \;\; d = 2$, the ripplet-I transforms as the transform of curvelet. These two factors enable the ripplet-I transform to accurately represent anisotropy, capturing 2D singularities along curves of diverse shapes. Next, they introduced the ripplet-II transform [50], which builds upon the generalized generalized random transform (GRT) [8, 9]; it aims to improve the capture of 2D singularities effectively, meeting requirements for multi-resolution, localization, and strong directionality with flexibility. Compared to wavelets and ridgelets, the ripplet-II transformation achieves the fastest coefficient reduction, resulting in a more compact representation of images with edges. Additionally, it exhibits rotational invariance, offering sparse feature vectors crucial for glaucoma detection. Consequently, it has been utilized in texture detection and image feature extraction tasks [50]. Due to its superior edge and texture capturing capabilities compared to conventional transforms, the ripplet-II transform is chosen for feature extraction in this study. This decision is motivated by the varied shapes of edges and textures present in the affected regions of fundus images.

3.2.1 Ripplet-II transform

Here, having a 2D function of g(x,y), and continious ripplet-II transform based on polar coordinates(ρ, α) can be specified on:

$$RT_g^2(s, t, \mathrm{d}, \theta) = \iint \tilde{\psi}_{s,t,\mathrm{d},\theta}\,(\rho, \alpha)\, g\,(\rho, \alpha)\, \rho\, \mathrm{d}\rho\, \mathrm{d}\alpha \tag{1}$$

Here, the $g(\rho, \alpha)$ shown as polar coordinate based on conversion by g(x,y),$\psi_{s,t,\mathrm{d},\theta}\Re^2 \rightarrow \Re^2$ is namely ripplet-II technique, $\tilde{\psi}$ has been as complex conjugte of ψ. Then, ripplet-II method defined by:

$$\psi_{s,t,\mathrm{d},\theta}\,(\rho, \alpha) = s^{-1/2}\varphi\left(\left(\rho cos^{\mathrm{d}}\left((\theta\;\alpha)\,/\mathrm{d}\right)\;t\right)/s\right) \tag{2}$$

Here, $\varphi : \Re \rightarrow \Re$ has been univariate of smooth wavelet method, $s > 0, t \in \Re, \mathrm{d} \in \mathbb{N}$ *and* $\theta \in |0, 2\pi)$ shows scale, translation, degree, orientation hyperparameters, accordingly. The ripplet-II transform is capable of encoding structural details along any given curve by tuning these hyperparameters using (1) and (2), specified as:

$$RT_g^2\,(s, t, \mathrm{d}, \theta) =< \varphi_{s,t}(\tau), GR_{\mathrm{d}}\,[g] > \tag{3}$$

Hence, $GD_{\mathrm{d}}[g]$ has the GDT function g and shown as:

$$GR_{\mathrm{d}}\,(\tau, \theta) = \iint g\,(\rho, \alpha)\,\delta\left(\tau \quad \rho\, cos^{\mathrm{d}}\,((\alpha\ \theta)\,/\mathrm{d})\right) \rho\, \mathrm{d}\rho\, \mathrm{d}\alpha \tag{4}$$

Hence, such GRT has been calculated based on Fourier transform [50] in (3) viewed as ripplet-II transform has the product of inner GRT, 1D- wavelet, which shows in :

$$g\,(\rho, \alpha) \overset{\mathrm{GRT}}{\Longrightarrow} GR_d[g]\,(\tau, \theta) \overset{\mathrm{1D-WT}}{\Longrightarrow} RT_g^2\,(s, t, \mathrm{d}, \theta) \tag{5}$$

Here, we have defined the ripplet-II transform, which works on two prime stages: firstly, evaluate the GRT based on g, after evaluating 1D WT on GRT using g. Using a nonlinear version of ripplet-II transform (DR2T), which is specified as:

$$g\,(\rho, \alpha) \overset{\mathrm{DGRT}}{\Longrightarrow} GR_d[g]\,(\tau, \theta) \overset{\mathrm{1D-DWT}}{\Longrightarrow} RT_g^2(s, t, \mathrm{d}, \theta) \tag{6}$$

Where a discrete GRT(DGRT) on g has been evaluated first, then 1D discrete WT (DWT) on DGRT of g has been evaluated. Based on a computational method using the discrete ripplet-II transforms, which is more straightforward if d=2. In such a case, the GRT has been dubbed 'parabolic Random transform', specified on [50].

$$GR_2\,(\tau, \theta) = 2\sqrt{\tau} R\left[g\left(\rho^{'2}.2\alpha^{'}\right)\right]\left(\sqrt{\tau}, \theta/2\right) \tag{7}$$

Here, $R\,[g\,(\rho, \alpha)]\,(\tau, \theta)$ utilizing the traditional random transform (CRT) in polar coordinates results in the Gaussian random transform (GRT) of function g for dimensions greater than zero, expressed in the Fourier domain:

$$\begin{gathered} GR_{\mathrm{d}}^F\,(\tau, \theta) = 2 \sum_{n=-\infty}^{+\infty} [\int_{\tau}^{\infty} \leq \int g\,(\rho, \alpha)\, e^{-in\,\alpha} \mathrm{d}\alpha \times \\ \left(1 - (\tau/\rho)^{2/\mathrm{d}}\right)^{-1/2} \times T_{nd}\left((\tau/\rho)^{1/\mathrm{d}}\right)] \mathrm{d}\rho e^{in\,\theta} \end{gathered} \tag{8}$$

Here, $T_n(.)$shows the polynomial of order n in the Chebyshev series. Finally, the assessment of a 2-dimensional forward DR2T applied to an input image can be expressed as:

1. Transform the input function from cartesian coordinates to polar coordinates, as follows $g\,(x, y)$ on $g\,(\rho, \alpha)$. Update (ρ, α) using $\left(\rho^{'2}, 2\alpha^{'}\right)$ on $g\,(\rho, \alpha)$. Hence, construct a new fundus image $g^{'}\,(x, y)$ employing interpolation following the conversion of polar coordinates $\left(\rho^{'}, \alpha^{'}\right)$ based on cartesian cordinates(x,y). Here, list of variables x, y store values of integer.
2. Deployed discrete CRT on $g^{'}\,(x, y)$ that generates and then substitue $R(\tau^{'}, \theta^{'})$ with $\left(\sqrt{\tau}, 0/2\right)$ in $R\left(\tau^{'}, \theta^{'}\right)$ as in (7). then obtain the DGRT coefficients $GR_2(\tau, \theta)$.
3. Consider a one-dimensional discrete wavelet transform (1D-DWT) to derive the discrete generalized Radon transform (DGRT) coefficients concerning the hyper-parameter τ and extract the discrete ripplet-II coefficients.

Therefore, the substitution mentioned earlier from $(\tau^{'}, \theta^{'})$ and $(\sqrt{\tau}, \theta/2)$ creates The coefficients of DR2T exhibit greater sparsity compared to those of other models.

3.2.2 Feature generation using DR2T

From our deployed work, DR2T has been utilized to extract features. We applied DR2T and obtained the coefficients for every training input glaucoma image. Next, the transform coefficients are arranged into a feature vector with a dimension of D, where D equals the product of m and n, representing the number of rows and columns in the image. This vector is generated for each training fundus image, forming a feature matrix. The Algorithm 1. outlines the methodology for implementing the feature generation process.

Algorithm 1 Feature extraction based on discrete ripplet-II tansform.

Input: fundus images $g[x, y]; 0 \le x < m, 0 \le y < n$
Output: Feature matrix F_M of size $N \times D$
1: **for** $eachfundusimageg\,[x, y] \in N$ **do**
2: Transform $g\,(x, y)$based on polar coordinates $g(\rho, \alpha)$, substitute the $(\rho, \alpha)\ with \left(\rho'^2, 2\alpha'\right)$
3: Transform coordinates of polar $\left(p', \alpha'\right)$ using coordinates of cartesian (x, y) which achieved another fundus image $g'\,(x, y)$ based on 2-D bi-linear has introduced
4: Evaluate 1-D FFT of $g'\,(x, y)$ that is $G'\,(u, v)$ with θ columns
5: Evaluate $GR_d\,(\tau, \theta)$ in Forurior domain which is $GR_d^F\,(\tau, \theta)$ for $G'\,(u, v)$ and d =2 based on (8)
6: Calcualte inverse of 1-D FFT $g_{inv}on\ GR_d^F\,(\tau, \theta)$ with θ columns
7: Implement 1-D DWT on g_{inv} with τ and get the coefficients. Sort the coefficients in a vector of size $1 \times D$ here. D is the sum of a list of features and is kept in a matrix
8: **end for**
9: Find out a feature matrix F_M having all vectors

3.3 Feature selection using meta-heuristic optimization techniques

Meta-heuristic optimization methods are adaptable algorithms employed for tackling a diverse array of intricate optimization challenges. They provide advantages such as handling various problems independently, conducting global searches, offering flexibility, ensuring computational efficiency, and maintaining resilience. There are several meta-heuristic techniques like gnetic algorithms (GA) [3], simulated annealing (SA) [20], PSO [28], ant colony optimization (ACO) [22] etc. In our suggested model, we have used golden jackal optimization (GJO) [10] for feature selection, which is crucially significant within the context of picking out the most significant image characteristics to decrease complexity and enhance the effectiveness of tasks. The GJO algorithm excels in efficiently addressing intricate optimization problems by harnessing the insights derived from the behaviour of jackals. Typical approaches involve using statistical measures and machine learning algorithms to preserve essential data while eliminating redundant information.

3.3.1 Golden jackal optimization algorithm

The GJO technique draws its motivation from golden jackals' hunting and feeding habits, serving as a meta-heuristic optimization approach. This approach seeks to replicate the versatile predators' adaptive hunting tactics, renowned for their capacity to flourish in a wide range of environments. GJO endeavours to tackle optimization problems efficiently and effectively [10]. It's following are the key steps in the search for a pair of golden jackals:

- Finding the target and moving closer to it.
- Catching the quarry and provoking it.
- Hunting down by capturing the prey.

With many meta-heuristic approaches, GJO utilizes a strategy centred around a population, commencing with an initial solution randomly distributed throughout the entire exploration region, as demonstrated in (9).

$$X_0 = X_{min} + rand * X_{max} - X_{min} \tag{9}$$

Here, X_{min} is denoted as the lower bound, X_{max} is specified as the upper bound and $rand$ shows a method that ranges from 0 to 1. Hence, (X_{prey}) is specified as the initial matrix Prey in (10). During the initialization phase, a pair of jackals emerged as the top two most fitness members in the group that was created.

$$X_{prey} = \begin{bmatrix} X_{1,1} & X_{1,2} & \dots & X_{1,q} \\ X_{2,1} & X_{2,2} & \dots & X_{2,q} \\ \vdots & \dots & \dots & \dots \\ X_{p,1} & X_{p,2} & \dots & X_{p,q} \end{bmatrix} \tag{10}$$

Equation (10) demonstrates, 'p' represents the prey, while 'q' represents the attributes. The position of every potential target mirrors the attributes of a specific outcome. The fitness method has been employed in optimization to evaluate the appropriateness at every target specified in (11). All the fitness values as the prey have been gathered within the matrics, using F matrics containing these elements for each prey. In this context, $X_{p,q}$ represents the p^{th} component of the q^{th} prey's dimension. The optimization problem pertains to a group of 'p' preys, which we denoted as the objective method as F. When researching the hunting behaviours of golden jackals, the main focus is on a male jackal, while the female jackal is considered a secondary fitness. The hunting pair collaboratively determines the locations of their prey, respectively.

$$\begin{bmatrix} f\left(X_{1,1}, X_{1,2}, \dots X_{1,q}\right) \\ f\left(X_{2,1}, X_{2,2}, \dots, X_{2,q}\right) \\ \vdots \\ f\left(X_{p,1}, X_{p,2}, \dots, X_{p,q}\right) \end{bmatrix} \tag{11}$$

Because of their inherent characteristics, jackals excel at detecting and chasing after prey. However, there are occasions when the prey manages to elude them, leading the jackals to explore other potential targets, a phase called the stage of exploration. While hunting, the male jackal assumes the role of the pack's leader, taking charge of the pursuit, with the female jackal closely trailing behind. Equations (12) and (13) Show the male jackal's location changing in each iteration, indicated by 'i'. The female jackal's location is denoted as XFM, while X represents the location of the male jackal, and $Xprey$ is viewed as the place of the prey. Based on the current location, the male jackal is referred to as X_1, while the adjusted location based on the female jackal as she pursues the prey is labelled as X_2. The energy the prey expands as it tries to escape is quantified as 'e' and is established using the following method in (14).

$$X_1 = X_M\,(i) - e|X_M\,(i) - s1 * X_{prey}(i)| \tag{12}$$

$$X_2 = X_{FM}\,(i) - e|X_{FM}\,(i) - s1 * X_{prey}(i)| \tag{13}$$

$$e = e_0 * e_1 \tag{14}$$

So, e_0 represents the initial energy level, while e_1 signifies the declining energy of the prey.

$$e_0 = 2 * \tau - 1 \tag{15}$$

$$e_1 = c_1 * \left(1 - \frac{i}{I}\right) \tag{16}$$

The variables in (15) and (16) consist of 'r,' a random integer with values ranging between 0 and 1, and 'c1,' which remains constant based on 1.5. In $'I'$, it shows on the maximum list of iterations, while 'i' stands for the ongoing iteration. Additionally, 'e1' experiences a gradual reduction from 1.5 to 0 as the iterations progress. Equations (12) and (13) deal with the calculation involves determining The gap separating the jackal from its target, viewed on $X(i) - s1 \times Xprey(i)$. Considering the prey's mysterious energy, the jackal's current position remains unchanged, with no addition or subtraction of distance. Two equations are utilized, with vector $s1$ generating a list of discrete values following its Levy distribution, representing the Levy position. To assess the prey's location based on the Levy sequence, this equation represents the vector $s1$ alongside the prey vector, which is visualized using (17).

$$s1 = 0.05 * LF(x) \tag{17}$$

In Levy flight technique, specified as $LF(x)$, has assessed based on (18) and (19). In this context, 'v' ranges from 0 to 1, and σ is established at 1.5.

$$LF(x) = \frac{0.05 * \sigma_\mu}{v^{\frac{1}{\sigma}}} \tag{18}$$

$$\sigma_\mu = \left[\frac{\tau(1+\sigma) * sin\left(\frac{\pi\sigma}{2}\right)}{\tau\left(\frac{1+\sigma}{2} * \sigma * 2^{\frac{\sigma-1}{2}}\right)}\right]^{\frac{1}{\sigma}} \tag{19}$$

In the end, Equation 20 specified as the new jackal positions are determined by averaging the results of the (12), (13).

$$X(i+1) = \frac{X_1(1) + X_2(i)}{2} \tag{20}$$

In our computational approach, we demonstrate the collaborative hunting behaviours of a male-female jackal through mathematical (21), (22). In this particular scenario, 'i' stands for the ongoing iteration, '$Xprey$' symbolizes the prey's position vector, '$XM(i)$' specified as the male jackal's location, '$XFM(i)$' represents based on the position of a female jackal. '$X_1(i)$' is the updated location based on the male jackal, while '$X_2(i)$' is the updated location of the female jackal based on prey; for updation, jackals' positions are specified by (14) and (20), that are used for calculating the prey's evasion energy. To prevent becoming trapped in local optima and encourage the pursuit of new possibilities, (21), (22) integrate on the '$s1$' method. In (17), assessing '$s1$' to reduce the likelihood of becoming trapped in suboptimal situations, particularly in the latter phases, mirrors the difficulties jackals encounter while hunting in their native environment. During the exploitation phase, '$s1$' grapples with these challenges.

$$X_1(i) = X_M(i) - e|s_1 * X_M(i) - X_{prey}(i)| \tag{21}$$

$$X_2(i) = X_{FM}(i) - e|s_1 * X_{FM}(i) - X_{prey}(i)| \tag{22}$$

Lastly, the GJO algorithm initiates by forming a randomized prey collection as a potential solution. In every cycle, the jackals work together to predict where their prey might be located. Within the group, each jackal updates the distances between pairs of jackals based on a preset rule. As time passes, the parameter e1 decreases gradually between 1.5 and 0 to achieve an equilibrium between pursuing new opportunities and utilizing existing resources. When the value of e surpasses 1, the golden jackal sets distance themselves based on prey. Conversely, e drops below 1, and the teams approach the target with more excellent proximity to improve their odds of capturing it.

3.3.2 Feature selection using golden jackal optimization algorithm (GJO)

The selection of features involves the deliberate choice of a more focused, smaller set of input variables selected from a more extensive dataset. Its main goal is to improve the precision of the ML scheme, reduce computational demands, and reduce the chances of overfitting. This technique aims to identify the most vital features that significantly influence the target variable. Selecting the appropriate features for classification can pose a challenge, and this is where GJO optimization comes into play. GJO optimization is used to identify a relevant subset of features. By utilizing GJO, we achieve a boost in classification accuracy. The subsequent segments comprehensively elucidate the distinct phases involved in GJO.

Initialization GJO employs a population-centric strategy, much like several other meta-heuristic techniques, wherein it uniformly explores the search space, commencing from the starting phase. The starting result specified in (23), In this context, X_{min} represents the minimum limit, X_{max} signifies the maximum limit, and 'rand()' is a method that produces values within the range of 0 to 1.

$$X_{inital} = X_{min} + rand().\,(X_{max} - X_{min}) \tag{23}$$

Suppose we have 'p' possible prey items and 'q' variables that each individual can exhibit, as outlined in the (24). In this context, 'i' ranges from 1 to 'p', with each 'i'' representing a single prey's position. Consequently, the prey groups can be represented based on 'p × q' vector denoted by $X_{prey} = \left(x_{ij}\right) p \times q$, as described, (25). Here, 'i' takes values $i = 1, 2, 3, 4 \ldots p$, and $j = 1, 2, 3, 4 \ldots q$, with each row representing an individual prey, and each column representing a specific variable or dimension. $X\,prey$ symbolizes the prey matrix established during initialization, comprising the two healthiest individuals, one male and one female jackal.

$$X_i = X_{i1} + X_{i2} + \ldots + X_{iq} \tag{24}$$

$$X_{prey} = X_{ij} = \begin{bmatrix} X_{1,1} & X_{1,2} & \ldots & X_{1,q} \\ X_{2,1} & X_{2,2} & \ldots & X_{2,q} \\ \vdots & \ldots & \ldots & \ldots \\ X_{p,1} & X_{p,2} & \ldots & X_{p,q} \end{bmatrix} \tag{25}$$

Utilizing an optimization approach involving a set of p prey entities and q variables, the arrangement of each prey element reveals the attributes of a specific solution. A performance evaluation function, also called a fitness function, is used to evaluate the effectiveness of every potential resolution during the optimization procedure. The results of this function for every possible solution have been documented in a matrix, as depicted in (26). In this equation, the variable 'i' ranges from 1 to 'p' and 'j' from 1 to 'q'. We capture the performance metrics for each prey in a matrix denoted as F_{ij}. The optimization procedure includes 'p' prey individuals, and their performance is evaluated using its designated objective function denoted as F_{ij}. Male jackals are regarded as the most skilled individuals in hunting, while their female counterparts are considered the second-most adept prey individuals. They are commonly referred to as male and female jackal prey positions.

$$F_{ij} = \begin{bmatrix} f\left(X_{1,1}, X_{1,2}, \ldots X_{1,q}\right) \\ f\left(X_{2,1}, X_{2,2}, \ldots, X_{2,q}\right) \\ \vdots \\ f\left(X_{p,1}, X_{p,2}, \ldots, X_{p,q}\right) \end{bmatrix} \tag{26}$$

Exploration phase In the golden jackal optimization (GJO) method, exploration has been achieved based on simulating the actions of a group of golden jackals as they forage for food in an unknown environment. Every jackal, representing a potential result, undergoes random movement based on the specified limits to enhance the search area; the random movement strategy prevents the algorithm from getting stuck in locally optimal solutions and promotes the discovery of novel solutions. Occasionally, the prey may elude capture, but jackals are naturally adept at sensing and tracking it. Consequently, when the prey proves elusive, the jackals explore to seek out alternative destinations. Throughout the hunt, the male jackal assumes the lead position, with the female jackal following closely behind. Equations (27) and (28) outline updating the male jackal's position in this pursuit. In this scenario, 'Xprey' signifies the vector indicating the prey's location, "X_M" represents the male jackal's location, while "XFM" signifies the female jackal's position. The instances 'i' denotes the recent iteration, while 'X_a' represents an updated location based on male jackal 'X_M'. 'X_b' is the position adjusted relative to the prey based on the jackal belonging to female groups 'X_{FM}'. To compute the prey's evasion energy, referred to as 'Ep,' (29) is applied. Within this equation, 'Ep0' is specified as the current energy of the prey, while 'E_{p1}' represents a reduction in its energy level.

$$X_a = X_M(i) - E_p|X_M(i) - s1 * X_{prey}(i)| \tag{27}$$

$$X_b = X_{FM}(i) - E_p|X_{FM}(i) - s1 * X_{prey}(i)| \tag{28}$$

$$E_p = E_{p0} * E_{p1} \tag{29}$$

Here, E_{p0} is determined by applying (30), and E_p1 is computed using (31). In these equations, we utilize the variable 'r,' a randomly generated number falling within the range of 0 to 1, along with a fixed value specified as 'c1,' set to 1.5. Furthermore, we introduce the variables 'I' to denote throughout the iterations and 'i' to represent the ongoing iteration count. The variable specified as decreasing energy of the prey is labelled as 'E_{p1}.' Its value gradually decreases based on 1.5 - 0, Expressing the gradual decline in the prey's energy.

$$E_p0 = 2 * \tau - 1 \tag{30}$$

$$E_{p1} = c_1 * \left(1 - \frac{i}{I}\right) \tag{31}$$

Equations (27) and (28) serve to calculate the jackal's distance based on prey, specified on $X(i) - s1 * X_{prey}(i)$. The jackal's positional adjustments are influenced by the prey's energy level, causing it to shift its position upwards or downwards depending on the proximity-based prey. By using vector s1, which is used in (27), (28) respectively, the sequence of unique values adheres to The Levy distribution, a unique probability distribution, is utilized to simulate Levy-type motion and is applied to represent the movement of the prey vector, mirroring Levy motion patterns. The calculation process for 's1' is explained in the following (32).

$$s1 = 0.05 * LF(x) \tag{32}$$

The levy flight method, represented as LF, has a computational formula to model stochastic movements within a defined search area. It finds common application in optimization algorithms, serving the same purpose in this scenario. The procedure includes generating random numbers conforming to the levy distribution and using them to modify the location of the search agent. The levy distribution is known for its prominent tails and is considered a probability distribution, enabling occasional substantial movements. Its quality proves advantageous in optimization assignments since it empowers search agents to venture into far-flung areas within the search space, which would be challenging to access through minor, gradual adjustments. The LF computed by applying (33), here 'u' and 'v' have sampled from its normal distribution based on standard deviations 'σ' and 'u' respectively. In this context, 'u' is a normal distribution characterized by a mean of σ_u and a variance of σ_v. On the other hand, 'v' follows a normal distribution based on the mean of μ derived from a normal distribution having mean with 0, variance σ_u^2, where, $u = normal\left(0, \sigma_u^2\right)$ and $v = normal\left(0, \sigma_v^2\right)$ The value of σ_u is determined on (34).

$$LF(x) = \frac{0.005 * u}{v^{\frac{1}{\sigma}}} \tag{33}$$

$$\sigma_\mu = \left[\frac{(1+\delta) * sin\left(\frac{\pi\delta}{2}\right)}{\frac{1+\delta}{2} * \delta * 2^{\frac{\delta-1}{2}}}\right]^{\frac{1}{\delta}} \tag{34}$$

Equation (35) is specified as the current position based on jackals' based on male and female specifications, considering the mean values derived from (27) and (28).

$$X(i+1) = \frac{X_a(i) + X_b(i)}{2} \tag{35}$$

Exploitation phase This phase replicates how a dominant male golden jackal leads a pack in hunting, gradually wearing down the prey until a male and female jackal duo can encircle it, leading to a swift capture. This collaborative hunting behaviour is mathematically shown in (36), (37), with 'i' denoting the current iteration. '$X_a(i)$' represents the male jackal's updated position, while '$X_b(i)$' describes the changed positions of the female jackal about its prey. To determine the prey's elusive vitality, labelled as 'E_p,' we apply (29), and subsequently, (35) is employed to reposition the jackals. In the exploitation phase, the utilization of 's1' is integrated into (36) and (37) to enhance exploration, reduce the likelihood of becoming trapped in local optimal solutions, and tackle issues similar to those encountered in actual hunting scenarios 's1' assists the jackals in converging toward the prey, particularly in later iterations.

$$X_a(i) = X_M(i) - E_P|s1 * X_M(i) - X_{pery}(i)| \tag{36}$$

$$X_b(i) = X_{FM}(i) - E_P|s1 * X_{FM}(i) - X_{pery}(i)| \tag{37}$$

Fitness and transfer function

The position matrix X_{prey} is converted from continuous values to binary values using a transfer function during fitness calculation and adjustments. In this particular research, a sigmoid transfer function has been presented in (38). The rationale behind selecting this sigmoid transfer function is its ability. It is essential to transition smoothly from real-number positions to binary values to optimise the algorithm's search efficiency and avoid premature convergence.

$$TF = \frac{1}{1 + e^{-X}} \tag{38}$$

From Equation, 'X' stands for the initial current position within its initial matrics, labelled 'X_{prey}, before transforming into a binary format. The sigmoid function is employed to convert the continuous input 'X' into a span ranging from 0 to 1, which allows for determining the appropriate binary representation. This conversion ensures that the position values are in binary format, making it easier to use them to compute the prey's fitness. Here, 'fitness' pertains to assessing a machine learning (ML) classifier's predictive accuracy. The 40% of the dataset is using for testing and rest 60% having training set. Then, the 'fitness' is determined by utilizing (39), where 'k' spans from 1 to 'm', where 'm' represents the quantity based on testing observations, then '$Err(k)$' denoted as prediction error based on 'k_{th}' observation. Then, the outcome was obtained by aggregating these errors and subsequently dividing them by 'm' to produce the mean prediction error.

$$fitness = \sum_{i=1}^{m} \frac{Err\ (k)}{m} \tag{39}$$

The algorithm uses two variables, MaleJackalscore and FemaleJackalscore, which show the fitness values based on its better-performing male with female jackals, which were identified as part of the optimization process. Here, the 'fitness' is specified as the fitness value, while MaleJackalscore and FemaleJackalscore serve as the updated fitness values. In this context, if the fitness level of a jackal, denoted as f, is less than the present MaleJackalscore, it indicates that the jackal possesses higher fitness than the current top male jackal. As a result, the position and performance of this jackal will replace those of the current male jackal. On the other hand, if a jackal's health is superior to MaleJackalscore but inferior to FemaleJackalscore, It implies a higher fitness level than the recent leading female jackal, which falls short of matching the fitness base of male jackal. In these instances, the current position and performance of the female jackal will be replaced by those of the new female jackal. After the fitness assessment, the resulting fitness will be expressed according to the (40), with the fitness array labelled as 'f_i,' comprising p elements, namely f_1, f_2, f_3, and so forth, up to f_p.

$$f_i = \left(f_1, f_2, f_3, \ldots, f_p\right) \tag{40}$$

Each algorithm step assigns a random value ranging from -1 to 1 to the initial energy, $Ep0$. $Ep0$ represents the physical strength of the prey, and reduced between 0 and -1 signifies the energy based on the prey's. On the other hand, an increase between 0 and 1 implies an improvement based on the prey's vitality. In contrast, a decline based on Ep becomes evident as the circular manner unfolds, depicted in Fig. 3. When the absolute magnitude that Ep exceeds 1, it signifies that the pairs of jackals are exploring various territories in search of prey, indicating that the Algorithm is currently in an exploratory stage. Conversely, here, the absolute magnitude based on Ep is < 1, then the Algorithm shifts into an exploitation stage, initiating predatory actions on the prey according to the Algorithm 2.

The GJO approach, crafted as a metaheuristic optimization method drawn from the hunting habits of golden jackals for inspiration, initiates by randomly populating prey. It pursues the best solution through multiple iterations, drawing parallels with jackals. In this analogy, the male jackal symbolizes the currently best solution, and the female jackal symbolizes

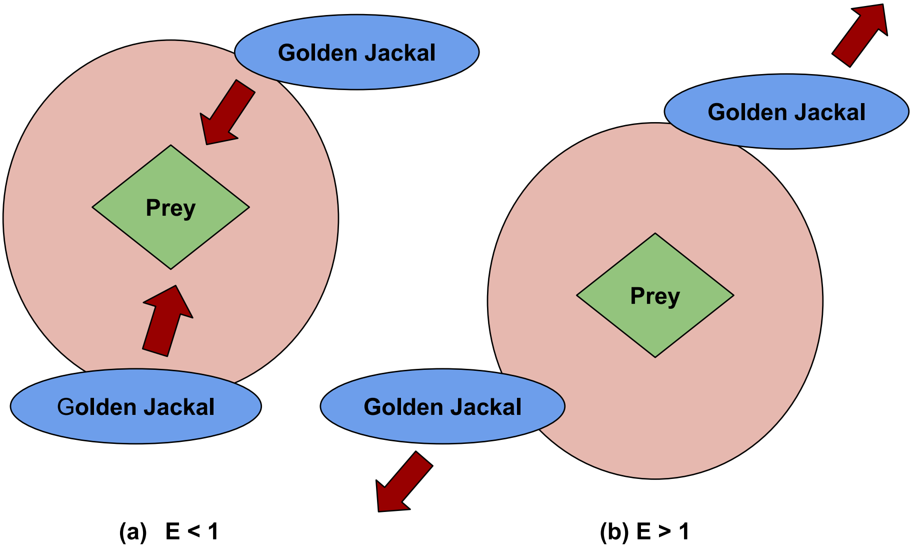

Fig. 3 Proposed algorithm GJO searching and attacking approches

Algorithm 2 The deployed GJO method for Algorithm.

Input: Initializing Randomly initiate the prey population as follows X_i is set for all i ranging from 1 to P, that is $X_i = (i = 1, 2, ..., P)$

while $i < I$ **do**
  Assume, position of male jackal as X_a
  Assume, Female Jackal position as X_b
  Assess the prey fitness value as
  if $fitness < MaleJackalscore$ **then**
    MaleJackalscore = fitness value
  end
  if $fitness > MaleJackalscore$ and $fitness < FemaleJackalscore$ **then**
    Do Set FemaleJackalscore = fitness
  end
  for $Eachprey$ **do**
    Using (29)-(31) update the evading energy E_p
    Update S1 by using (32) and (33)
    if $E \geq 1$ **then**
      Then Exploitation stage
    end
  end for
  Revise the prey's location based on the provided (27), (28) and (35)
  if $E < 1$ **then**
    Then Exploration stage
  end
  Modify the prey location based on (35) - (37)
  Update Jackal Position, $X(i) = \frac{X_a + X_b}{2}$
  By employing a transfer method to transform continuous scores of Xi uisng (38)
  $i{+}{+}$
end while
Revert to the male jackal's Position X_a

the second-best choice. The algorithm subsequently fine-tunes every target's location and evasive energy by employing specific equations designed for the purpose. Subsequently, it proceeds with either exploration or exploitation based on the evasion energy value. The algorithm changes the jackal's location by determining the average of the positions of both males and females. Subsequently, it alters ongoing prey position scores into binary equivalents through a specified transformation function. This repetitive procedure persists for a predefined number of iterations, ultimately yielding the male jackal's position, representing the optimal outcome achieved throughout its execution. This process provides a deeper insight into the GJO algorithm, based on Algorithm 3 for a detailed explanation and Fig. 4 for a visual depiction in a flowchart.

3.4 Classification using LS-SVM

In fundus image classification, machine learning classifiers are used to label data, a crucial aspect of supervised learning. There are several classifiers like XGBoost [39], Random Forest

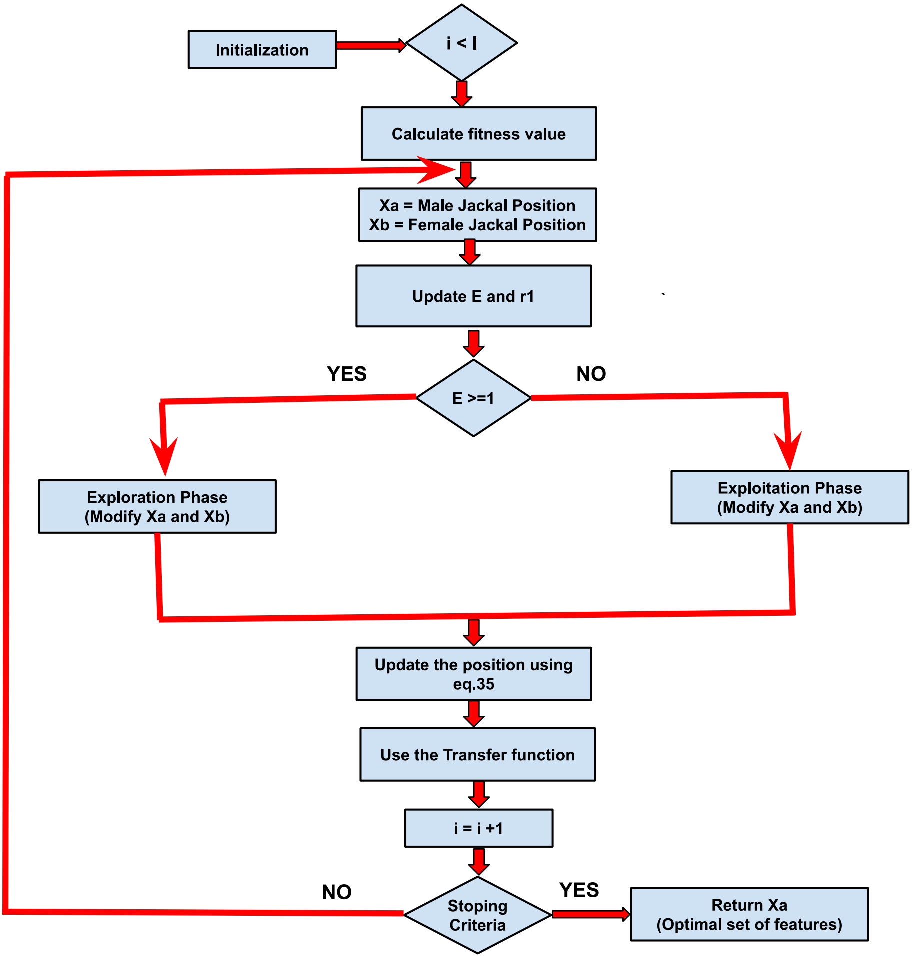

Fig. 4 Flowchart of the proposed algorithm

(RF) [31], Decision Trees (DT) [40], k-nearest neighbour (KNN) [26], and back-propagation neural network (BPNN) [26] with distinct applications and performance characteristics. In our proposed work, we have used LS-SVM to classify glaucoma fundus images.

Conventional SVM poses a substantial computational burden when handling large-dimensional datasets. To address this computational complexity, this paper employs an updated variant known as LS-SVM, which has been employed as glaucoma detection. Unlike the standard SVM, which involves solving a quadratic programming problem, LS-SVM addresses a collection of linear equations because it uses equality constraints in its formulation [33]. In (41), provided with a training dataset consisting of N data points represented as $\{x_k, d_k\}_{k=1}^{N}$ for k ranging from 1 to N, where each $x_k \in k^m$ belongs to a space of dimension m and each $d_k \in \{-1, +1\}$ is a class label taking values from, Formulating LS-SVM as an optimization problem specified as follows:

$$\min_{w_i b_i, e} J(\omega, b, e) = \frac{1}{2}\omega^T \omega + \zeta \frac{1}{2}\sum_{k=1}^{N} e_K^2 \tag{41}$$

Hence, the quality constant defined as follows

$$d_k \left[\omega^T \varphi(x_k) + b\right] = 1 - e_k, \quad k = 1, 2, \ldots, N \tag{42}$$

In (42), ω specified as weight vector $\varphi(.)$ shown as mapping method, $\zeta > 0$ called the factor of regularization, b assigned as the bias and e_k specifed as variables error. The Lagrangian can be specified as

$$\iota(\omega, b, e, \alpha) = J(\omega, b, e) - \sum_{k=1}^{N} \alpha_k \left\{d_k \left[\omega^T \varphi(x_k) + b\right] - 1 + e_k\right\} \tag{43}$$

Here, φ_k is specified as multipliers language. The optimality conditions in (43) shown as $\frac{\delta \pounds}{\delta \omega} = 0 \rightarrow \omega = \sum_{k=1}^{N} \alpha_k d_k \varphi(x_k)$; $\frac{\delta \pounds}{\delta b} = 0 \rightarrow \sum_{k=1}^{N} \alpha_k d_k = 0$; $\frac{\delta \pounds}{\delta \alpha_k} = 0| \rightarrow \alpha K = \zeta e_k; and \frac{\delta \pounds}{\delta \alpha_k} = 0 \rightarrow d_k\left[\omega^T \varphi(x_k) + b\right] - 1 + e_k = 0$, that specified as result of the corrosponding list of linear Equations.

$$\begin{bmatrix} I & 0 & 0 & -Z^T \\ 0 & 0 & 0 & X_D^T \\ 0 & 0 & \zeta^{-}I & -I \\ Z & D & I & 0 \end{bmatrix} = \begin{bmatrix} \omega \\ b \\ e \\ \alpha \end{bmatrix} = \begin{bmatrix} 0 \\ 0 \\ 0 \\ \vec{1} \end{bmatrix} \tag{44}$$

Here, $Z = \left[\varphi(x1)^T \ d_1 \ldots; \varphi(xN)^T \, dN\right], D = [d_1; \ldots; d_N], \vec{1} = [1; \ldots; 1], e = [e_1; \ldots; e_N], \alpha = [\alpha 1; \ldots \alpha N]$. We have find the result as

$$= \begin{bmatrix} 0 & -D^T \\ D & \Omega + \zeta^{-}1I \end{bmatrix} \begin{bmatrix} b \\ \alpha \end{bmatrix} = \begin{bmatrix} 0 \\ \vec{1} \end{bmatrix} \tag{45}$$

Here, $\Omega = ZZ^T$ and based on Mercer's condition [47],

$$\Omega_{kl} = d_k d_l \zeta(x_k)^T \ \varphi(x_1) = d_k d_l K(x_k, x_l) \tag{46}$$

Hence, $K(., \ldots\ldots)$ is the kernel method. From LS-SVM algorithm can be achieved based on:

$$f(x) = sign\left[\sum_{k=1}^{N} \alpha_k \, d_k K(x, x_K) + b\right] \tag{47}$$

In kernel functions applied to train the classifier have been tabulated in Table 2. The hyperparameter θ is shown as a polynomial degree, and σ is the free hyperparameter that manages the kernel's size.

Algorithm 3 Pseudocode based on employed system.

Offline learning 1:
for all $eachgroundthruthfundusimage$ **do**
Improve the visual contrast using CLAHE Implement DR2T with degree 2 on the improved image Achived the DR2T coefficients and form a feature vector set with dimension D
end for
Ensure: Glaucoma or healthy fundus images.
Step 1: Feature generation using DR2T
2: Apply GJO method to decrease the dimension of feature vector from D to Xa
3: Specify k-fold stratified cross validation on all the entire dataset and generate the training and testing data
4: Feed reduced feature set to the LS-SVM algorithm training to predict detection of glaucoma performance
5: Evaluate it's classification result on the test set
Online prediction 6: Load the unknown glaucoma fundus image as input
7: pre-processing the query image with CLAHE
8: Achived the DR2T based on degree 2 based on the enhanced fundus image
9: Evaluate the reduced feature vector by applying the GJO method
10: Feed reduced feature set as LS-SVM model based on kernel K to predict on test data as glaucoma or healthy

4 Experimental results and discussion

The experiments were performed on the PARAM Shavak, a powerful supercomputer featuring a tabletop setup with a high-performance computing (HPC) system. It is equipped with an Intel(R) and Xeon(R) Gold 5220R CPU operating at a speed of 2.20GHz. The system is designed with an approximate of CPUs with two multicore, which have a minimum of 12 cores. Additionally, it incorporates one or two GPU accelerator cards, such as the NVIDIA with K40 accelerator card and NVIDIA based on P5000. It provides a system with peak computing power of 3 Tera-Flops, accompanied by 8 TB of storage and 64 GB of RAM. Additionally, it is embedded based on a pre-installed parallel programming development environment and possesses computing power of 2 TF and above. We conducted our experiments using the computer-aided diagnosis (CAD) model we proposed and implemented using Python 3.9.6. In our deployed work, we have considered two standard datasets, namely, G1020 [2] and ORIGA [53]. Here, we have divided the glaucoma datasets into a 60%(training) and 40%(testing) ratio to achieve the highest level of accuracy. The experiments have been configured with specific parameters like σ set at 1.5, the population size is 30, and the values of maximum iteration is 200 tabulated in Table 3. Similarly, the hyperparameters lists used for various classifiers have been tabulated in Table 4. We've utilized

Table 2 Several Kernel techniques applied on LS-SVM

List of Kernels	Defination
Linear	$K(\infty, \infty_k) = \infty_K^T \infty$
Polynomial	$K(\infty, \infty_k) = \left(\infty_K^T \infty + 1\right)^{\theta}$
Radial Basis Function (RBF)	$K(\infty, \infty_k) = exp\left\{-\|\|\infty - \infty_k\|\|^2/2\sigma^2\right\}$

Table 3 Parameters utlized in GJO feature selection models

Parameters	Values
Population size	30
Maximum iteration	200
r (Random integer)	0 to 1
c1(Constant value), σ	1.5

a five-fold stratified cross-validation (SCV)approach to address overfitting concerns. This technique splits the dataset into five distinct subparts, observing that no overlapping occurs. Next, the model underwent training using four subsets, assessed on the remaining portion. The iterative method has continued five times, with each iteration serving based on evaluation at least once. Employing such a scheme improves the model's performance and helps prevent overfitting. The five-fold SCV using a single run has been shown in Fig. 5.

4.1 Preprocessing and feature extraction results

To increase the contrast based on the initial glaucoma fundus image, the CLAHE method is used, and the settings of its parameters influence its performance. In this scenario, the initial

Table 4 Hyperparameters for different classifiers

Algorithms	Specifications	Parameters
XGBoost [39]	Learning rate	0.3
	n-estimators	100
	Scale-pos-wirght	1
Random Forest [31]	n-estimators	100
	Criterion	Gini
	Min-impurity-decrease	0
	Number of folds	5
Decision Tree [40]	Criterion	Gini
	Max-features	0,1
	Min-sample-leaf	1
	Min-sample-split	2
KNN [26]	Nearest neighbors(K)	1
	Nearset neighbor search algorithm	Euclidean distance
	List of folds	5
BPNN [26]	Learning rate, momentum	0.001, 0.4
	Hidden neurons	6
	List of folds	5
LS-SVM Linear [18]	Dimension space	$-1, +1$
	Kernel type	Linear
	List of folds	5
LS-SVM Polynomial [18]	Order	2
	Kernel type	Poly
	List of folds	5
LS-SVM RBF [18]	θ, σ	[1-10]
	Kernel type	RBF
	List of folds	5

Poly-Polynomial, RBF-Radial basis function kernel

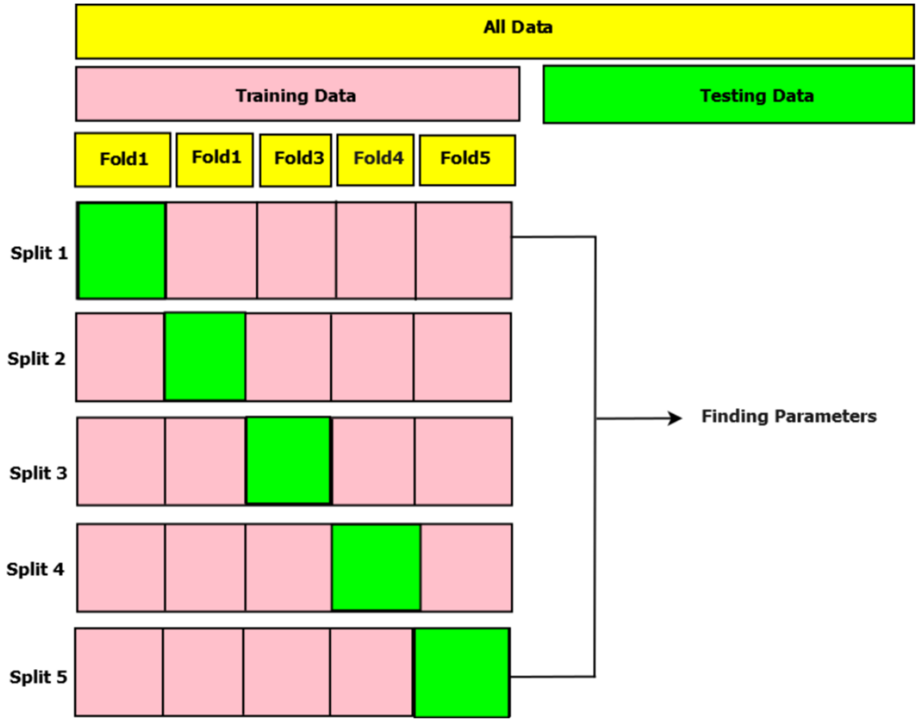

Fig. 5 Allocation of sample sets for each experiment through the utilization of k-Fold Stratified Cross-Validation

fundus image is partitioned into 64 distinct contextual regions, with 256 bins and a clip limit (β) of 0.01 have been selected. It's important to highlight that a uniform distribution approach is applied to each region to achieve a consistent flat histogram shape. Subsequently, we apply the DR2T technique to each preprocessed image, extracting features as transform coefficients using a 2-level 1D DWT with the Haar wavelet chosen as the basis because of its straightforward nature. Since the sum of glaucoma fundus images has been obtained, the dimensions of $256 \times 256 = 65536$. Hence, instead of DR2T, we employ 2D DWT and ridglet transform and have preserved their coefficients. The procedure entails determining the magnitude of the coefficients for each change and then normalizing them according to the most crucial coefficient. The normalized coefficients' magnitudes are then arranged in descending order to assess the rate of reduction in coefficients, as illustrated in Fig. 6. Notably, DR2T outperforms 2D DWT and ridgelet in terms of the speed at which coefficients decline. Consequently, DR2T generates sparse feature vectors that notably improve classification accuracy.

4.2 Feature selection results

Here, we have implemented an improved scheme for feature selection, which involves using the GJO algorithm. This approach leverages metaheuristic optimization with the GJO algorithm to effectively identify the most optimal set of features, i.e., (29 features) from discrete

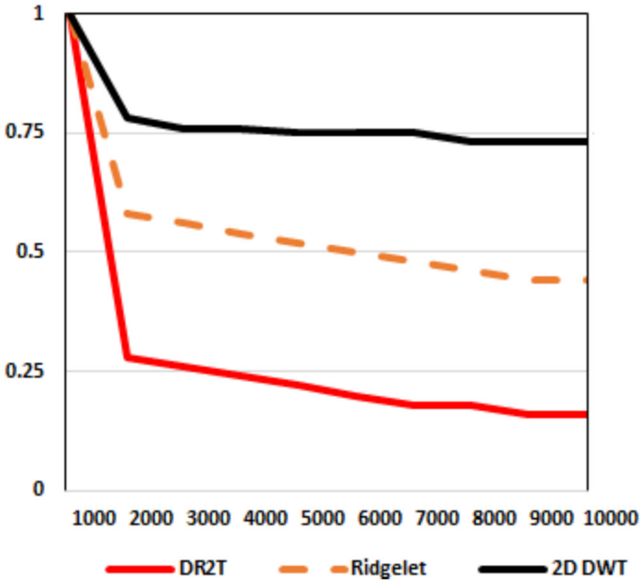

Fig. 6 Cofficient decaying comparision with list of image transform

ripplet-II transform (DR2T). Feature selection helps mitigate collinearity, leading to more stable coefficient estimates and improved model accuracy. From our experimental analysis, we have obtained better classification results on both datasets. Namely G1020 [2], and ORIGA [53] by selecting 29 features. The proposed model DR2T+GJO+LS-SVM+RBF provides better classification accuracy with 29 optimal features. Also, we have compared the effectiveness of our employed scheme with feature selection without feature selection. Table 5 presents a comparative analysis of the proposed model and LS-SVM using various kernels, with and without GJO, in terms of accuracy, sensitivity, and specificity (in %) on the G1020 and ORIGA datasets. We have compared the list of features based on their respective classification accuracy, and the comparison graphs have been shown in Figs. 7 and 8. Our experimental results show that our deployed model DR2T+GJO+LS-SVM+RBF gives better classification accuracy with 29 optimal features in both datasets.

Table 5 Comparative analyses (%) of the proposed model with LS-SVM with list of kernels and LS-SVM with kernels+GJO method

Proposed Method	No. of feature	G1020			ORIGA		
		A_{cc}	S_{en}	S_{pe}	A_{cc}	S_{en}	S_{pe}
DR2T+LS-SVM+Linear	32	91.42	88.14	92.76	94.62	94.03	94.82
DR2T+LS-SVM+Polynomial	32	92.16	88.98	93.45	95.38	91.04	96.89
DR2T+LS-SVM+RBF	32	92.65	91.53	93.10	96.15	94.03	96.89
DR2T+GJO+LS-SVM+Linear	29	92.63	90.60	93.45	95.77	95.52	95.82
DR2T+GJO+LS-SVM+Polynomial	29	93.14	90.68	94.14	96.54	96.37	97.01
DR2T+GJO+LS-SVM+RBF	**29**	**93.38**	**92.37**	**93.79**	**97.31**	**97.01**	**97.41**

A_{cc}-Accuracy, S_{en}-Sensitivity, S_{pe}-Specificity

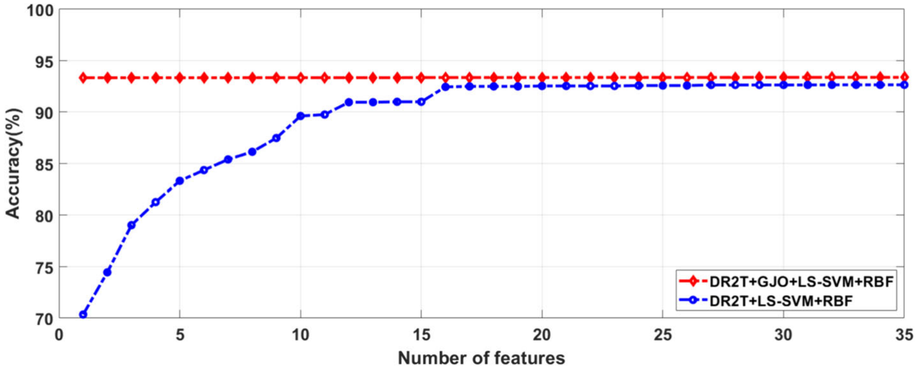

Fig. 7 Classification result obtained in G1020 dataset has exprimented with least number of features

4.3 Classification results

We have utilized LS-SVM with several kernels for glaucoma detection during our classification. We have assessed how well our suggested model performs using three parameters: accuracy, sensitivity and specificity. Here, we have considered two standard datasets: G1020 [2] and ORIGA [53]. To improve the quality of our dataset, we applied a cropping process to extract relevant regions of interest (ROI). Ophthalmologists provided the CDR scores on numerous images. Our approach primarily centred on cropped images resized at 256 × 256 pixels. In cases where specific ROIs were unavailable due to a lack of prior information, all 256 × 256 images have been considered. We have divided our whole dataset into training sets and testing sets based on the ratio 60%, 40% accordingly. The training and testing sample details have been specified in Table 1, and some samples of the dataset set have been shown in Fig. 2. We have deployed by assessing the classification performance through a five-fold stratified cross-validation procedure involving ten iterations. We manually fine-tuned the model's hyper-parameters to extract high-level features. Then, the LS-SVM was the prime classifier for our classification task. We have used different traditional classifiers like XGBoost [39], RF [31], DT [40], KNN [26], and BPNN [26] with accuracy 90.93%, 89.22%, 88.97%, 91.18%, 91.67% accordingly in the G1020 dataset. Like the ORIGA dataset, several algorithms, namely, XGBosst, RF, DT, KNN, and BPNN, have an accuracy of 91.41%, 90.63%, 89.84%, 93.44%, 93.46%. The comparison of all existing classifiers with our deployed scheme is

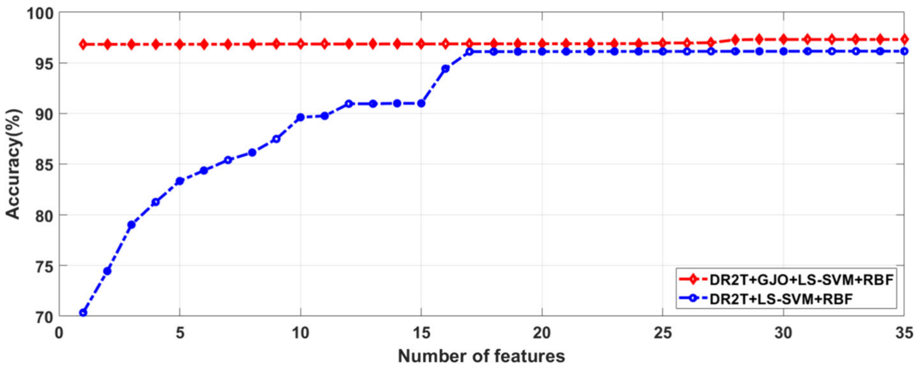

Fig. 8 Classification result obtained in ORIGA dataset has examined with least number of features

Table 6 Comparative analysis (%) of deployed model with Glaucoma datasets

Classifiers	G1020 Dataset			ORIGA Dataset		
	A_{cc}	S_{en}	S_{pe}	A_{cc}	S_{en}	S_{pe}
XGBoost	90.93	87.29	92.41	91.41	88.89	92.23
RF	89.22	83.90	91.38	90.63	87.38	91.71
DT	88.97	86.97	90.00	89.84	85.84	91.19
KNN	91.18	87.29	92.76	93.44	92.54	93.75
BPNN	91.67	89.83	92.41	93.46	89.55	94.82
DR2T+GJO+LS-SVM+RBF(Proposed)	**93.38**	**92.37**	**93.79**	**97.31**	**97.01**	**97.41**

A_{cc}: Accuracy, S_{en}: Sensitivity , S_{pe}: Specificity

tabulated in Table 6. Furthermore, to showcase the enhanced performance of DR2T features in comparison to DWT, curvelet (FDCT) features, we have carried out an experiment in which we have separately utilized DWT and FDCT features within the proposed system, and the outcomes can be found from Table 7. During classification results, we observed that our suggested scheme produced superior classification accuracy at 93.38% and 97.31 %, having the G1020 and ORIGA datasets, accordingly. Table 8, 9, 10 and 11 represents the details of 5-fold SCV results of both the datasets. The AUC results of different kernels obtained by the false positive rate concerning the true positive rate on both the G1020 and ORIGA datasets are shown in Figs. 9 and 10. Then, The confusion matrix of both datasets, namely G1020 and ORIGA, is shown in Fig. 11. Figures 12 and 13 show the performance comparison of the various classifiers on both datasets.

During our experimental analysis, we have observed that our employed model DR2T+GJO +LS-SVM+RBF achieved better classification results than existing models with less number of features. Hence, we have contrasted conventional LS-SVM with different kernels like linear, polynomial and radial basis function (RBF). From the experimental results, we have observed that the LS-SVM with RBF kernel has achieved better classification results with less number of features as compared to other existing models. For feature selection we have used GJO to select optimal features. These simulated results have been conducted on two standard datasets, namely G1020 and ORIGA datasets. The efficacy of the proposed model has been determined by two different experiments, without feature selection techniques and with feature selection techniques. Both the experimental results have been shown in the Table 7.

4.4 Compariosn with other state-of-the-art models

We have conducted experiments to evaluate our new model, comparing it to previous models. We have compared our proposed model with traditional CAD techniques to gauge its effec-

Table 7 Comparative result(%) based on wavelet and curvlet based on G1020 and ORIGA dataset

Schemes	No. of features	Dataset (A_{cc} in (%)	
		G1020	ORIGA
DWT+LS-SVM	32	90.20	91.92
DWT+GJO+LS-SVM	32	91.42	94.23
FDCT+GJO+LS-SVM	32	91.98	95.38
DR2T+GJO+LS-SVM	**29**	**93.38**	**97.31**

Table 8 Glaucoma classifcation of average outcomes (%) of suggested DR2T without GJO method using G1020 dataset for 5-fold 10 times for DR2T+LS-SVM+RBF kernel

R	$F_N - 1$	$F_N - 2$	$F_N - 3$	$F_N - 4$	$F_N - 5$	A_{cc}
1	92.65	92.65	92.65	92.63	92.63	92.64
2	92.65	92.65	92.65	92.65	92.63	92.65
3	92.65	92.65	92.65	92.63	92.63	92.64
4	92.65	92.65	92.65	92.65	92.63	92.65
5	92.65	92.65	92.65	92.63	92.65	92.65
6	92.65	92.65	92.63	93.65	93.65	92.65
7	92.65	92.65	92.63	92.63	92.63	92.64
8	92.65	92.65	92.65	92.65	92.63	92.65
9	92.65	92.65	92.65	92.65	92.63	92.65
10	92.65	92.65	92.65	92.63	92.65	92.65
Final Result						**92.65 ± 0.0045**

F_N: Fold Number, R: Run, A_{cc}: Average Accuracy

tiveness. The evaluation results we conducted with G1020 and ORIGA fundus images have been tabulated in Table 12. Our proposed model obtained better detection of outcomes than existing models, even with fewer features. This represents a significant advantage compared to various CAD models for identifying glaucoma. While the increase in accuracy is modest and similar to specific existing methods, it's worth noting that this outcome was achieved across multiple iterations of a k-fold stratified cross-validation procedure, underscoring the robustness and dependability of the proposed approach.

4.5 Advantages and disadvantages of proposed model

The experimental outcomes shows that the proposed model improves the classification results as compared to other existing models with less number of features. The proposed model uses discrete ripplet-II transform (DR2T) for extraction of features. Compared to other transforms

Table 9 Glaucoma classification of average outcomes (%) of suggested DR2T with GJO method using G1020 dataset for 5-fold 10 times for DR2T+GJO+LS-SVM+RBF kernel

R	$F_N - 1$	$F_N - 2$	$F_N - 3$	$F_N - 4$	$F_N - 5$	A_{cc}
1	93.30	93.30	93.30	93.63	93.63	93.43
2	93.30	93.30	93.30	93.63	93.63	93.43
3	93.30	93.30	93.30	93.3	93.3	93.30
4	93.30	93.30	93.30	93.63	93.63	93.43
5	93.30	93.30	93.30	93.63	93.63	93.43
6	93.30	93.30	93.30	93.30	93.30	93.30
7	93.30	93.30	93.30	93.63	93.63	93.43
8	93.30	93.30	93.30	93.30	93.30	93.30
9	93.30	93.30	93.30	93.63	93.63	93.43
10	93.30	93.30	93.30	93.30	93.30	93.30
Final Result						**93.38 ± 0.0636**

F_N: Fold Number, R: Run, A_{cc}: Average Accuracy

Table 10 Glaucoma classifiction of average outcomes(%) of employed DR2T without GJO method uisng ORIGA dataset for 5-fold 10 times for LS-SVM+RBF kernel

R	$F_N - 1$	$F_N - 2$	$F_N - 3$	$F_N - 4$	$F_N - 5$	A_{cc}
1	96.03	96.03	96.27	96.27	96.27	96.17
2	96.03	96.03	96.27	96.27	96.27	96.17
3	96.03	96.03	96.03	96.03	96.27	96.08
4	96.27	96.27	96.27	96.03	96.03	96.17
5	96.03	96.03	96.27	96.27	96.27	96.17
6	96.03	96.03	96.03	96.03	96.27	96.08
7	96.03	96.03	96.27	96.27	96.27	96.17
8	96.27	96.27	96.27	96.03	96.03	96.17
9	96.03	96.03	96.27	96.27	96.27	96.17
10	96.03	96.03	96.03	96.03	96.27	96.08
Final Result						**96.15 ± 0.0017**

F_N: Fold Number, R: Run, A_{cc}: Average Accuracy

namely discrete wavelet transform (DWT), Fourier transform, ridgelet, lifting wavelet transform (LWT), etc., DR2T has produced 2D singularities with arbitrarily shaped curves, which are available in the fundus images. Also, it obtains rotation invariant, sparse features, which is important for improving the detection problem. Here, the golden Jackel optimization (GJO) algorithm has been utilized for selecting the optimal features with reduced feature dimensions and improve the model's accuracy.

Our proposed model DR2T+GJO+LS-SVM+RBF integrates feature extraction, feature selection, and classification based on advanced machine learning techniques to achieve high performance, improved accuracy, and efficiency in processing complex datasets. Our simulation results have focused on the discrete ripplet-II transform (DR2T) that captures multi-directional and anisotropic details in fundus images more effectively than traditional transforms, which is crucial for identifying subtle glaucoma features. Then, the optimal features have been selected by meta-heuristic optimization techniques called golden jackal

Table 11 Glaucoma classification of average outcomes (%) of employed DR2T with GJO method using ORIGA dataset for 5-fold 10 times for DR2T+GJO+LS-SVM+RBF kernel

R	$F_N - 1$	$F_N - 2$	$F_N - 3$	$F_N - 4$	$F_N - 5$	A_{cc}
1	97.31	97.30	97.31	97.31	97.31	97.31
2	97.31	97.30	97.31	97.31	97.31	97.31
3	97.30	97.30	97.30	97.30	97.30	97.30
4	97.31	97.31	97.31	97.31	97.31	97.31
5	97.31	97.31	97.31	97.31	97.31	97.31
6	97.30	97.30	97.30	97.30	97.30	97.30
7	97.31	97.31	97.31	97.31	97.31	97.31
8	97.31	97.31	97.30	97.31	97.31	97.31
9	97.31	97.31	97.30	97.31	97.31	97.31
10	97.30	97.30	97.30	97.30	97.30	97.30
Final Result						**97.31 ± 0.0045**

F_N: Fold Number, R: Run, A_{cc}: Average Accuracy

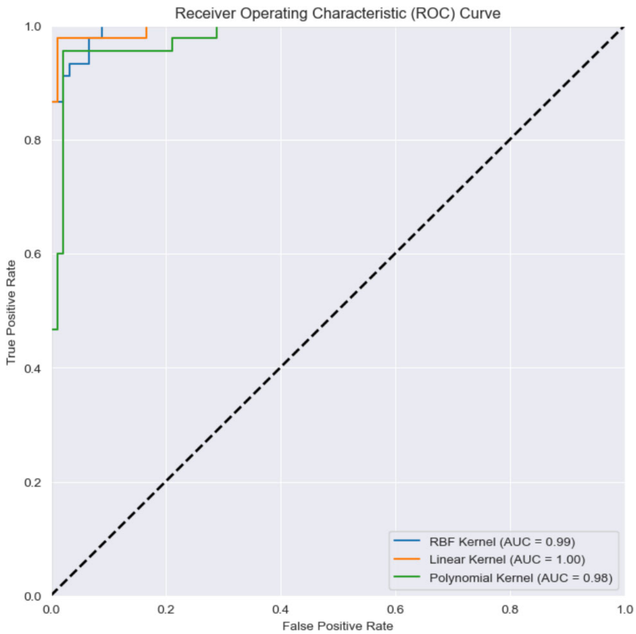

Fig. 9 The AUC curves for LS-SVM classifierwith three kernels using G1020 dataset

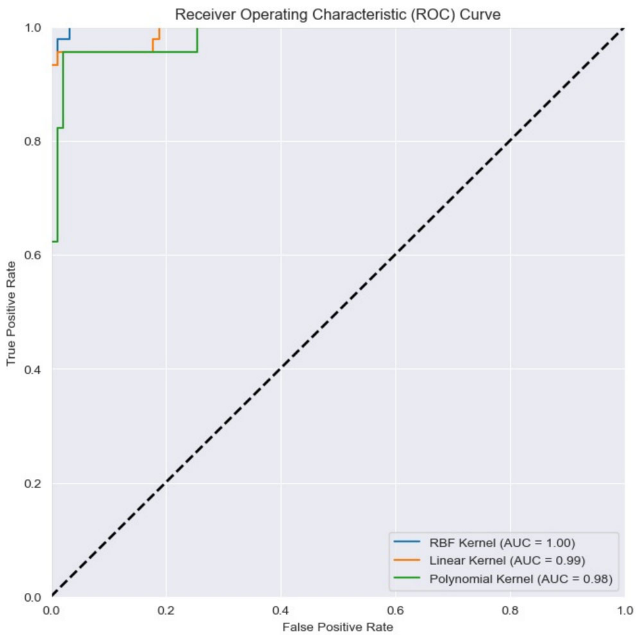

Fig. 10 The AUC curves for LS-SVM classifierwith three kernels using using ORIGA dataset

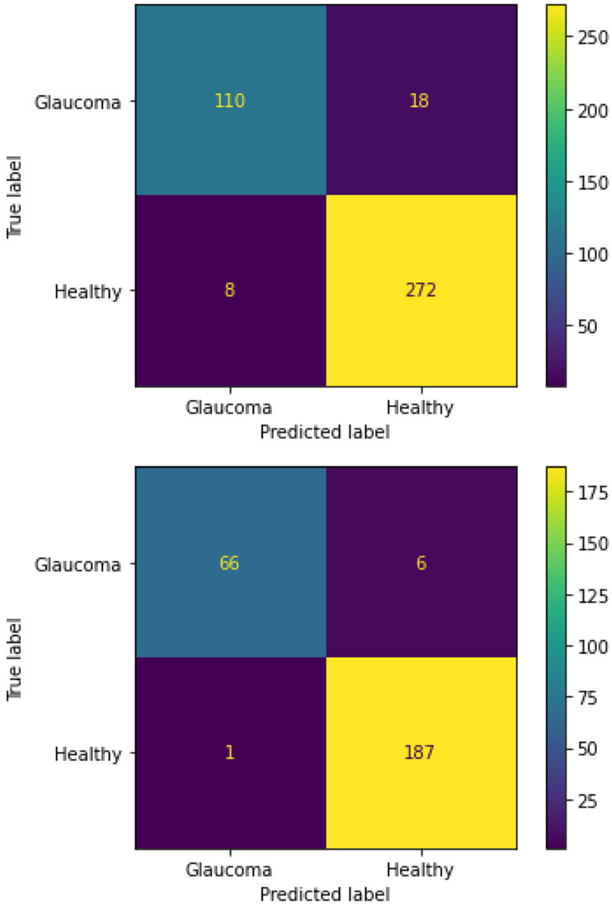

Fig. 11 Confusion matrix of proposed model visualized on G1020 and ORIGA Datasets

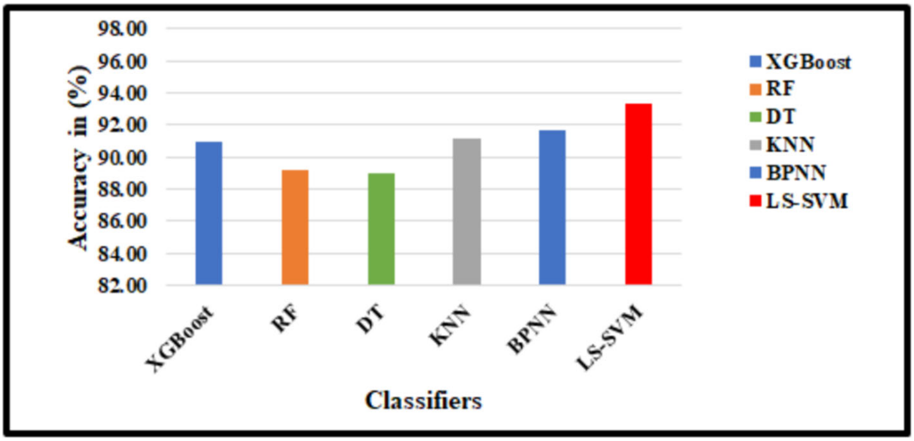

Fig. 12 Classification accuracy achieved by various classifiers with proposed scheme using G1020 dataset

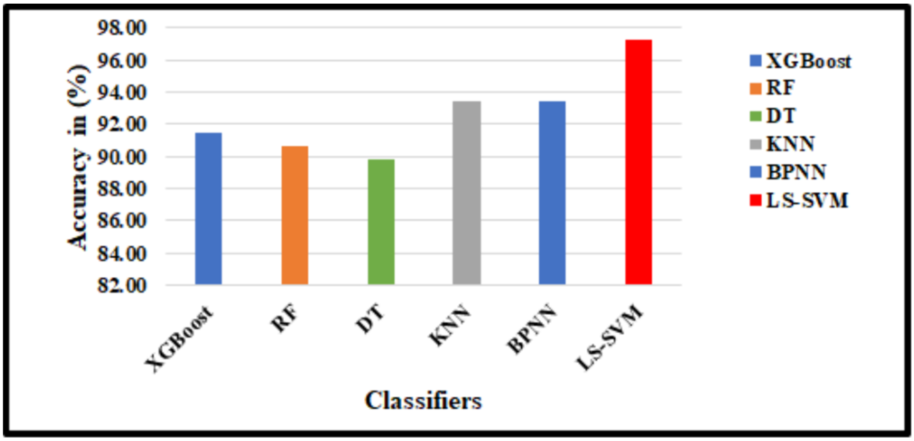

Fig. 13 Classification accuracy achieved by various classifiers with proposed scheme using ORIGA dataset

optimization (GJO), which reduces computational load and enhances the model's performance. Finally, we have utilized the least square support vector machine (LS-SVM) to provide accurate and robust classification by solving a more straightforward optimization problem than standard SVMs, leading to more precise glaucoma detection. Our model, combining high-quality feature extraction with optimized feature selection, minimizes the chances of misclassification, improving the reliability of glaucoma detection. The combined DR2T and metaheuristic optimization approach ensures the system can efficiently handle large datasets, making it scalable for widespread clinical use. The advanced feature extraction and selection process adapts well to the variability in fundus images, providing consistent performance across diverse patient data. Overall, this integrated method enhances glaucoma detection's accuracy, efficiency, and reliability in fundus images by leveraging sophisticated feature extraction and optimization techniques coupled with novel machine-learning approaches. Still, the proposed model has several demerits, as follows. The proposed model has been experimented with only retinal fundus images. We can test our model with other images like optical coherence tomography (OCT) images, confocal scanning laser ophthalmoscopy (CSLO) images, etc. The proposed model solves binary classification problems, but multi-

Table 12 Performance simulation on proposed method with existing CAD shemes using G1020 and ORIGA datasets

Existing Schemes	A_{cc} (%)	
	Datasets	
	G1020	ORIGA
2D-FBSE-EWT [7]	–	91.01
SMOTE+RF [54]	–	78.30
SMOTE+SVM [54]	–	82.80
HOG+SVM [1]	83.32	–
HOG +PNN [1]	87.92	–
HOG+RNN [1]	85.72	–
DR2T+GJO+LS-SVM+RBF(Proposed Model)	**93.38**	**97.31**

A_{cc}- Accuracy

class classification is challenging. However, the GJO requires more number of parameters to tune, so in future, we can use other optimisation techniques with less number of parameters.

4.6 Discussion and summary

Our experiments demonstrated the visualization capabilities of input fundus images using CLAHE and extracted features with discrete ripplet-II transform (DR2T). The golden jackal optimization algorithm (GJO) has been employed to reduce feature dimensionality. We used a least square support vector machine (LS-SVM) with linear, polynomial, and radial basis function (RBF) kernels for classification. The employed work classified fundus images as glaucoma or healthy and has been validated on two standard datasets namely G1020 and ORIGA. Our proposed model DR2T+GJO+LS-SVM+RBF achieved better classification results of 93.38 % for G1020 and 97.31 % for ORIGA with 29 features. However, our experimental results show that performance heavily relies on selecting an appropriate kernel function, which can be challenging and subjective despite the model's benefits in improving detection accuracy.

- The proposed model utilized fewer parameters for effective feature learning, and features obtained through the discrete ripplet-II transform (DR2T).
- The golden jackal optimization algorithm (GJO) has been utilized to minimize feature dimensionality
- For classification, we have utilized a least square support vector machine (LS-SVM) with linear, polynomial, and radial basis function (RBF) kernels.
- Our proposed model deployed on detection of glaucoma fundus images as glaucoma or healthy and validated using the G1020 and ORIGA datasets.
- Our employed model DR2T+GJO+LS-SVM-RBF achieved better classification accuracy, which is 93.38% for the G1020 dataset and 97.31% for the ORIGA dataset, with a reduced number of features.
- The proposed model attains superior classification accuracy while using fewer features compared to existing models

Consequently, this method can be a supplementary tool for early glaucoma detection and improve clinical recommendations.

5 Conclusions and future scope

The paper presented a novel approach to glaucoma detection in fundus images by leveraging the discrete ripplet-II transform (DR2T) for feature extraction and a metaheuristic algorithm named GJO for feature selection, combined with least square support vector machine (LS-SVM) for classification. The key contributions and findings include: firstly, the discrete ripplet-II transform effectively captured the intricate structural details of fundus images, providing robust features that enhance the discrimination between glaucoma and healthy images. Secondly, for feature selection, we have employed golden jackal optimization algorithm (GJO) metaheuristic algorithms, explicitly improving the efficiency of the feature selection process. These algorithms optimized the selection of the most relevant features, reducing the dimensionality of the dataset while retaining essential information for accurate classification. Finally, LS-SVM with RBF kernel applied to classify the image as glaucoma or healthy. The findings from the experiments on two publicly available datasets, namely G1020 and ORIGA, show that the suggested method achieves greater classification accuracy than other competent methods, even when using a minimal number of features. In the future, the proposed model's overall performance could be enhanced by employing advanced feature extraction and selection techniques. Deep learning could be investigated as a vital alternative to the deployed scheme, and hybridizing fewer parameters based on different optimization techniques can be another work in the future.

Author Contributions Santosh Kumar Sharma: Conceptualization, Methodology, Investigation, Writing- Original draft preparation, Software. Debendra Muduli: Supervision, Validation, Writing - Review and Editing. Adyasha Rath: Validation, Resources and Editing. Sujata Dash: Validation, Resources and Editing. Ganapati Panda: Validation, Resources and Editing. Achyut Shankar: Validation, Resources and Editing. Dinesh Chandra Dobhal: Validation, Resources and Editing.

Funding The authors declare that no funds, grants, or other support were received during the preparation of this manuscript.

Data Availability Data will be made available on request.

Declarations

Conflicts of interests The authors declare that they have no known competing financial interests or personal relationships that could have appeared to influence the work reported in this paper.

References

1. Ananya S, Bharamagoudra MR, Bharath K, Pujari RR, Hanamanal VA (2023) Glaucoma detection using hog and feed-forward neural network. In: 2023 IEEE International Conference on Integrated Circuits and Communication Systems (ICICACS), IEEE, pp 1–5
2. Bajwa MN, Singh GAP, Neumeier W, Malik MI, Dengel A, Ahmed S (2020) G1020: A benchmark retinal fundus image dataset for computer-aided glaucoma detection. In: 2020 International Joint Conference on Neural Networks (IJCNN), IEEE, pp 1–7
3. Balasubramanian K, Ananthamoorthy NP (2022) Correlation-based feature selection using bio-inspired algorithms and optimized kelm classifier for glaucoma diagnosis. Appl Soft Comput 128(109):432
4. Candes E, Demanet L, Donoho D, Ying L (2006) Fast discrete curvelet transforms. Multiscale Model Sim 5(3):861–899
5. Candès EJ, Donoho DL (1999) Ridgelets: A key to higher-dimensional intermittency? Philos Trans R Soc London Series A Math Phys Eng Sci 357(1760):2495–2509
6. Candès EJ, Donoho DL et al (1999) Curvelets: A surprisingly effective nonadaptive representation for objects with edges. Department of Statistics, Stanford University, Stanford, CA, USA
7. Chaudhary PK, Pachori RB (2021) Automatic diagnosis of glaucoma using two-dimensional fourier-bessel series expansion based empirical wavelet transform. Biomed Signal Process Control 64(102):237
8. Cormack A (1982) The radon transform on a family of curves in the plane. ii. Proc Am Math Soc 86(2):293–298
9. Cormack AM (1981) The radon transform on a family of curves in the plane. Proc Am Math Soc 83(2):325–330
10. Das H, Prajapati S, Gourisaria MK, Pattanayak RM, Alameen A, Kolhar M (2023) Feature selection using golden jackal optimization for software fault prediction. Mathematics 11(11):2438
11. Do MN, Vetterli M (2003) The finite ridgelet transform for image representation. IEEE Trans Image Process 12(1):16–28
12. Drance S, Anderson DR, Schulzer M, Group CNTGS et al (2001) Risk factors for progression of visual field abnormalities in normal-tension glaucoma. Am J Ophthalmol 131(6):699–708
13. Fu H, Cheng J, Xu Y, Zhang C, Wong DWK, Liu J, Cao X (2018) Disc-aware ensemble network for glaucoma screening from fundus image. IEEE Trans Med Imaging 37(11):2493–2501
14. Garway-Heath D, Hitchings R (1998) Quantitative evaluation of the optic nerve head in early glaucoma. Br J Ophthalmol 82(4):352–361

15. Gautam D (2024) Improved machine learning-based glaucoma detection from fundus images using texture features in fawt and ls-svm classifier. Multimedia Tools and Applications pp 1–16
16. Ghahremani M, Ghassemian H (2014) Remote sensing image fusion using ripplet transform and compressed sensing. IEEE Geosci Remote Sens Lett 12(3):502–506
17. Islam MT, Imran SA, Arefeen A, Hasan M, Shahnaz C (2019) Source and camera independent ophthalmic disease recognition from fundus image using neural network. In: 2019 IEEE International Conference on Signal Processing, Information, Communication & Systems (SPICSCON), IEEE, pp 59–63
18. Kar NB, Babu KS, Sangaiah AK, Bakshi S (2019) Face expression recognition system based on ripplet transform type ii and least square svm. Multimed Tools Appl 78:4789–4812
19. Kausu T, Gopi VP, Wahid KA, Doma W, Niwas SI (2018) Combination of clinical and multiresolution features for glaucoma detection and its classification using fundus images. Biocybern Biomed Eng 38(2):329–341
20. Kubecka L, Jan J (2004) Registration of bimodal retinal images-improving modifications. In: The 26th Annual International Conference of the IEEE Engineering in Medicine and Biology Society, IEEE, vol 1, pp 1695–1698
21. Kumar R, Kumbharkar P, Vanam S, Sharma S (2024) Medical images classification using deep learning: a survey. Multimed Tools Appl 83(7):19683–19728
22. Larabi-Marie-Sainte S, Alskireen R, Alhalawani S (2021) Emerging applications of bio-inspired algorithms in image segmentation. Electronics 10(24):3116
23. Latif J, Tu S, Xiao C, Bilal A, Ur Rehman S, Ahmad Z (2023) Enhanced nature inspired-support vector machine for glaucoma detection. Comput Mater Contin 76(1)
24. Maheshwari S, Pachori RB, Acharya UR (2016) Automated diagnosis of glaucoma using empirical wavelet transform and correntropy features extracted from fundus images. IEEE J Biomed Health Inform 21(3):803–813
25. Maheshwari S, Pachori RB, Kanhangad V, Bhandary SV, Acharya UR (2017) Iterative variational mode decomposition based automated detection of glaucoma using fundus images. Comput Biol Med 88:142–149
26. Muduli D, Dash R, Majhi B (2020) Automated breast cancer detection in digital mammograms: a moth flame optimization based elm approach. Biomed Signal Process Control 59(101):912
27. Muduli D, Dash R, Majhi B (2021) Enhancement of deep learning in image classification performance using vgg16 with swish activation function for breast cancer detection. In: Computer Vision and Image Processing: 5th International Conference, CVIP 2020, Prayagraj, India, December 4-6, 2020, Revised Selected Papers, Part I 5, Springer, pp 191–199
28. Muduli D, Dash R, Majhi B (2021) Fast discrete curvelet transform and modified pso based improved evolutionary extreme learning machine for breast cancer detection. Biomed Signal Process Control 70(102):919
29. Muduli D, Dash R, Majhi B (2022) Automated diagnosis of breast cancer using multi-modal datasets: a deep convolution neural network based approach. Biomed Signal Process Control 71(102):825
30. Muduli D, Kumar RR, Pradhan J, Kumar A (2023) An empirical evaluation of extreme learning machine uncertainty quantification for automated breast cancer detection. Neural Comput Appl 1–16
31. Muduli D, Priyadarshini R, Barik RC, Nanda SK, Barik RK, Roy DS (2023b) Automated diagnosis of breast cancer using combined features and random forest classifier. In: 2023 6th International Conference on Information Systems and Computer Networks (ISCON), IEEE, pp 1–4
32. Nayak AB, Shah A, Maheshwari S, Anand V, Chakraborty S, Kumar TS (2024) An empirical wavelet transform-based approach for motion artifact removal in electroencephalogram signals. Decis Anal J 100420
33. Nayak DR, Dash R, Majhi B (2015) Least squares svm approach for abnormal brain detection in mri using multiresolution analysis. 2015 International Conference on Computing. Communication and Security (ICCCS), IEEE, pp 1–6
34. Parashar D, Agrawal DK, Tyagi PK, Rathore N (2022) Automated glaucoma classification using advanced image decomposition techniques from retinal fundus images. In: AI-Enabled Smart Healthcare Using Biomedical Signals, IGI Global, pp 240–258
35. Pisano ED, Zong S, Hemminger BM, DeLuca M, Johnston RE, Muller K, Braeuning MP, Pizer SM (1998) Contrast limited adaptive histogram equalization image processing to improve the detection of simulated spiculations in dense mammograms. J Digit Imaging 11:193–200
36. Pizer SM (1990) Contrast-limited adaptive histogram equalization: Speed and effectiveness stephen m. pizer, r. eugene johnston, james p. ericksen, bonnie c. yankaskas, keith e. muller medical image display research group. In: Proceedings of the first conference on visualization in biomedical computing, Atlanta, Georgia, vol 337, p 2

37. Raghavendra U, Bhandary SV, Gudigar A, Acharya UR (2018) Novel expert system for glaucoma identification using non-parametric spatial envelope energy spectrum with fundus images. Biocybern Biomed Eng 38(1):170–180
38. Raja C, Gangatharan N (2015) A hybrid swarm algorithm for optimizing glaucoma diagnosis. Comput Biol Med 63:196–207
39. Raju M, Shanmugam KP, Shyu CR (2023) Application of machine learning predictive models for early detection of glaucoma using real world data. Appl Sci 13(4):2445
40. Rodríguez-Robles F, Verdú-Monedero R, Berenguer-Vidal R, Morales-Sánchez J, Sellés-Navarro I (2023) Analysis of the asymmetry between both eyes in early diagnosis of glaucoma combining features extracted from retinal images and octs into classification models. Sensors 23(10):4737
41. Sanghavi J, Kurhekar M (2024) Ocular disease detection systems based on fundus images: a survey. Multimed Tools Appl 83(7):21471–21496
42. Sharma SK, Priyadarshi A, Mohapatra SK, Pradhan J, Sarangi PK (2022) Comparative analysis of different classifiers using machine learning algorithm for diabetes mellitus. In: Meta Heuristic Techniques in Software Engineering and Its Applications: METASOFT 2022, Springer, pp 32–42
43. Sharma SK, Zamani AT, Abdelsalam A, Muduli D, Alabrah AA, Parveen N, Alanazi SM (2023) A diabetes monitoring system and health-medical service composition model in cloud environment. IEEE Access 11:32804–32819
44. Sharma SK, Muduli D, Priyadarshini R, Kumar RR, Kumar A, Pradhan J (2024) An evolutionary supply chain management service model based on deep learning features for automated glaucoma detection using fundus images. Eng Appl Artif Intell 128(107):449
45. Shyla NJ, Emmanuel WS (2021) Automated classification of glaucoma using dwt and hog features with extreme learning machine. In: 2021 third international conference on intelligent communication technologies and virtual mobile networks (ICICV), IEEE, pp 725–730
46. Singh A, Dutta MK, ParthaSarathi M, Uher V, Burget R (2016) Image processing based automatic diagnosis of glaucoma using wavelet features of segmented optic disc from fundus image. Comput Methods Programs Biomed 124:108–120
47. Suykens JA, Vandewalle J (1999) Least squares support vector machine classifiers. Neural Process Lett 9:293–300
48. Wang W, Zhou W, Ji J, Yang J, Guo W, Gong Z, Yi Y, Wang J (2022) Deep sparse autoencoder integrated with three-stage framework for glaucoma diagnosis. Int J Intell Syst 37(10):7944–7967
49. Xavier FJ (2024) Odmnet: Automated glaucoma detection and classification model using heuristically-aided optimized densenet and mobilenet transfer learning. Cybern Syst 55(1):245–277
50. Xu J, Wu D (2012) Ripplet transform type ii transform for feature extraction. IET Image Process 6(4):374–385
51. Xu J, Yang L, Wu D (2010) Ripplet: A new transform for image processing. J Vis Commun Image Represent 21(7):627–639
52. Yin F, Lee BH, Yow AP, Quan Y, Wong DWK (2016) Automatic ocular disease screening and monitoring using a hybrid cloud system. In: 2016 IEEE international conference on Internet of Things (iThings) and IEEE green computing and communications (GreenCom) and IEEE cyber, physical and social computing (CPSCom) and IEEE smart data (SmartData), IEEE, pp 263–268
53. Zhang Z, Yin FS, Liu J, Wong WK, Tan NM, Lee BH, Cheng J, Wong TY (2010) Origa-light: An online retinal fundus image database for glaucoma analysis and research. In: 2010 Annual international conference of the IEEE engineering in medicine and biology. IEEE, pp 3065–3068
54. Zhao X, Guo F, Mai Y, Tang J, Duan X, Zou B, Jiang L (2019) Glaucoma screening pipeline based on clinical measurements and hidden features. IET Image Process 13(12):2213–2223

Authors and Affiliations

Santosh Kumar Sharma[1] **· Debendra Muduli**[1] **· Adyasha Rath**[1] **· Sujata Dash**[2] **· Ganapati Panda**[1] **· Achyut Shankar**[3,4,5,6,7] **· Dinesh Chandra Dobhal**[7]

✉ Debendra Muduli
muduli.debendra@gmail.com

Santosh Kumar Sharma
santoshsilu84@gmail.com

Adyasha Rath
adyasha.rath@cgu-odisha.ac.in

Sujata Dash
sujata@nagalanduniversity.ac.in

Ganapati Panda
ganapati.panda@gmail.com

Achyut Shankar
ashankar2711@gmail.com

Dinesh Chandra Dobhal
dineshdobhal@geu.ac.in

1 Department of Computer Science and Engineering, C.V. Raman Global University, Odisha, India

2 Department of Information Technology, School of Engineering and Technology, Nagaland University, Dimapur, India

3 Department of Cyber Systems Engineering, WMG, University of Warwick, Coventry CV74AL, UK

4 University Centre for Research & Development, Chandigarh University, Mohali, Punjab 140413, India

5 School of Computer Science Engineering, Lovely Professional University, Phagwara 144411, Punjab, India

6 Center of Research Impact and Outcome, Chitkara University, Rajpura, Punjab, India

7 Department of Computer Science & Engineering, Graphic Era Deemed to be University, Dehradun, Uttarakhand 248002, India